Cement and Concrete Research 197 (2025) 107967

Contents lists available at ScienceDirect

Cement and Concrete Research

journal homepage: www.elsevier.com/locate/cemconres

The dissolution of fly ashes in undersaturated alkaline solutions

Yujia Min, Lisa E. Burris *

Department of Civil, Environmental and Geodetic Engineering, Ohio State University, Columbus, OH 43210, USA

ARTICLE INFO

Keywords:
Dissolution
Fly ash
Reactivity
NBO/T
R3

ABSTRACT

This study investigated the dissolution of 8 class C and 8 class F fly ashes in undersaturated conditions at pH 12.4–13.8 and 25–60 °C. Class C fly ashes showed preferential dissolution of Al over Si, while congruent dissolution was observed for low Ca fly ashes. Si in solution inhibited the dissolution of class C ashes, while Ca and Al inhibited the dissolution of class F ashes. NaOH dissolved class F fly ashes faster than KOH at the same concentrations. Non-bridging oxygen per tetrahedra correlated with dissolution rates in early hours while long-term reactivity was related to reactive Al and Si content. Dissolution in the dilute solution was consistent with reaction extent in R^3 mixtures at 25 °C, and but greater for reactions at 40 and 60 °C. These results help us understand fly ash dissolution and predict reactivity under conditions relevant to those used to evaluate performance in cementitious mixtures.

1. Introduction

Fly ashes are commonly used supplementary cementitious materials that replace a portion of a concrete mixture's portland cement content and can alter fresh and later age properties, including improving long-term durability performance [1,2]. However, the supply of traditional fly ashes for which current specifications, e.g. ASTM C618 [3] and AASHTO M295 [4], were developed is in decline due to the reduction in coal energy production [5]. New sources of fly ashes, including harvested fly ash sources, are being successfully utilized [6,7], but better understanding of the reactions of fly ash in concrete mixtures, and the extent to which novel test methods assess this parameter are essential in order to evaluate the suitability of these new ash sources for use in concrete. Thus, in order to enable rapid assessment of fly ash quality and mitigate the gaps between the supply and demand for fly ashes in the concrete industry testing methods must be developed that effectively evaluate the performance of fly ashes [8]. One of the key aspects of the performance of fly ashes is their reactivity [1], which has been shown to correlate with their contribution to concrete mechanical strengths [9] and durability, including the mitigation of alkali-silica reactions [10]. To ensure that reactive materials are allowed for use in concrete while prohibiting non-reactive materials a comprehensive understanding of the reactions of fly ash in cementitious materials is needed.

The dissolution of fly ashes is a critical step during their reaction in cementitious mixtures [11]. The dissolution of Ca-aluminosilicate glasses, one of the main components of fly ash glasses [12–14], has been found to usually occur faster in coal ashes with higher Ca/(Al + Si) glass ratios [13,15–17]. This observation was explained by the structure of silicate glasses: the dissolution process is controlled by the breakdown of the glass tetrahedron network formed by Al and Si connected by bridging oxygens. The presence of network modifiers, like Ca, can lead to the depolymerization of the network and facilitate the breakdown of the network: a higher depolymerization degree results in more bridging oxygens becoming non-bridging oxygens. Thus, an index called non-bridging oxygen per tetrahedron (NBO/T) has been used to predict the dissolution rates of silicate glasses [11]. However, recent studies have found that the effects of glass structure on glass dissolution kinetics cannot be solely explained by NBO/T [12,18], but are also affected by reactive surface area, the development of diffusion barriers due to the coverage of glasses particles surfaces by the hydrates formed during pozzolanic reactions, and varying environmental conditions such as solution chemistry and temperature [1,19].

The dissolution of silicate glasses and minerals has been modeled as a function of surface area, temperature, aqueous species, and chemical affinity, which can be summarized as Eq. 1 [20]:

$$\textit{Dissolution rate} = S \times A \times e^{\frac{-E_a}{RT}} \times a_i^{n_i} \times \left(1 - \frac{Q}{K}\right)^{\sigma} \quad (1)$$

where S is the reactive surface area in m^2, A is a pre-exponential factor in $mol{\cdot}m^{-2}{\cdot}s^{-1}$, E_a is the activation energy in $J{\cdot}mol^{-1}$, R is the gas constant in $J{\cdot}mol^{-1}{\cdot}K^{-1}$, T is temperature in Kelvin. The exponential term $e^{-Ea/RT}$

* Corresponding author at: 211A Bolz Hall, 2070 Neil Ave, Columbus, OH 43210, USA.
E-mail address: burris.189@osu.edu (L.E. Burris).

https://doi.org/10.1016/j.cemconres.2025.107967
Received 12 March 2025; Received in revised form 22 May 2025; Accepted 10 June 2025
Available online 18 June 2025
0008-8846/© 2025 Elsevier Ltd. All rights are reserved, including those for text and data mining, AI training, and similar technologies.

describes the dependency of dissolution rate on temperature. The product of A and $e^{-Ea/RT}$ is also called the rate constant, k. a_i is the activity of aqueous species that affect the kinetics of dissolution such as H^+ and OH^-, Na^+, and K^+ [20]. The impact of these aqueous species is usually modeled using power indexes n_i. When a_i is H^+ or OH^-, the corresponding indexes n_H and n_{OH} are also called pH dependency factors. Dissolution rates are usually a function of the chemical affinity of the dissolution reaction. The chemical affinity describes how close the reaction is to the equilibrium, and is a function of Q, the ion activity product (unitless). Q increases with the activities of reaction products, which in fly ash systems are primarily Ca, Al, and Si species released into solution during dissolution. K is an equilibrium constant (unitless). Sometimes a Temkin coefficient σ will be needed to fit the experimental results. The activities of aqueous species close to the dissolving solid surfaces could be different from those in bulk solutions if diffusion barriers have developed around the particles. While silicate glass and minerals are extensively studied, experimental evaluation of these parameters for fly ashes is scarce.

Considering these factors, the dissolution kinetics of fly ashes are likely significantly different under varying conditions. Indexes solely based on elemental compositions, such as NBO/T, may be useful for a rough quality assessment, but additional testing is needed to understand the reactivity of fly ashes under all conditions [2,14]. In addition, the fly ash system is even more complicated because it is a mixture of many different glasses and crystalline phases [6,21]. Our current understanding of fly ash dissolution is not comprehensive enough to accurately predict dissolution kinetics and more information on the dissolution behaviors of fly ashes including rates, activation energies, and effects of solution chemistry, is needed before accurate models can be built to predict the reactivities of fly ashes and the meaning of existing reactivity test methods' results understood.

To gain more information on the fly ash dissolution process, dissolution tests were conducted using 8 class C and 8 class F commercially-available fly ashes with a widely varying chemical compositions, intended to reflect a broad range of fly ashes which may be used in concrete mixtures, in diluted alkaline solutions. The impacts of solution chemistry, temperature, pH, and ionic strength on the dissolution kinetics were elucidated to provide additional information needed for modeling fly ash reactivity. The relationships between NBO/T, dissolution rates and reactive content were explored to understand the impact of ash chemical composition on the fly ash reactivity in early stage and long term. The differences between the fly ash dissolution in undersaturated conditions and that in cementitious mixtures, simulated by R^3 mixtures, were also examined in order to improve understanding of the contribution of dissolution to fly ash reactions in cementitious systems, as well as better understand the meaning of R^3 reactivity testing results. The outcomes provide insights into the factors controlling the reactivity of fly ashes and will aid in development of more accurate models of the fly ash dissolution-reaction process occurring in fly ash-concrete systems.

2. Materials and methods

2.1. Materials

Sixteen coal combustion fly ashes were obtained from Eco Materials Technologies, the SEFA Group, and Titan America. The elemental compositions were characterized using X-ray fluorescence spectroscopy (XRF), as shown in Table 1. Fly ashes investigated in this study were classified into 8 Class C and 8 Class F ashes according to ASTM C618. The available alkali (Na_2O_e = Na_2O + 0.658 K_2O) were determined following ASTM C311 procedures. The amorphous contents were characterized using X-ray diffraction (XRD). The phase compositions and particle size distributions characterized using laser diffraction (LS-13-320, Beckman Coulter) are provided in the Supporting Information.

Sodium hydroxide, potassium hydroxide, calcium hydroxide, aluminum hydroxide, potassium silicate, potassium chloride, sodium chloride, and potassium sulfate were obtained from Fisher Scientific. All chemicals were at least ACS grade and solutions were prepared using ultra-purified water (18.2 MΩ-cm, Milli-Q).

2.2. Dissolution tests

Dissolution behaviors of fly ashes were tested at 25, 40, and 60 °C, using a solid-to-liquid ratio of 0.1 g/L. The pH was adjusted using KOH or NaOH. The solutions were mixed and their temperature was controlled using a magnetic stirring hotplate. The samples, collected during the experiments, were filtered using 0.22 μm filters, diluted in 2 % nitric acids, and analyzed using inductively coupled plasma-optical emission spectrometry (ICP-OES). Replicate tests were conducted on selected samples (Fig. S2) and the error range of dissolved ion concentrations was ~ ± 10 %.

2.3. Calculation of activation energy, pH dependency, and NBO/T

The activation energies, which represent the dependency of dissolution kinetics on the temperature were calculated using the slopes when plotting -ln(k) against the 1/RT. The rate constant k was estimated using the slopes when plotting $1-(1-\alpha)^{1/3}$ with time (α is dissolved fraction) [22]. Description of the procedures used to calculate activation energy, dissolved fractions of the samples, variation in dissolution rate, and normalized dissolution rates can be found in the supplemental information. This shrinking core model considers the evolution of spherical particle surfaces along the progress of dissolution. However, actual fly

Table 1
Elemental compositions, available alkali, and amorphous content of fly ashes.

wt%	SiO_2	Al_2O_3	Fe_2O_3	CaO	MgO	SO_3	Na_2O	K_2O	TiO_2	P_2O_5	Na_2O_e	Amorphous content
C1	40.36	18.56	4.56	19.91	3.67	0.80	1.43	0.56	1.04	1.05	1.31	77.8
C2	31.36	14.60	4.97	24.77	6.89	2.18	1.91	0.33	0.90	1.18	1.64	60.0
C3	36.70	22.82	4.53	22.45	4.33	1.19	3.44	0.95	1.28	1.09	1.49	83.6
C4	27.66	22.88	4.23	21.54	4.52	2.55	12.61	0.76	1.27	0.67	5.05	89.8
C5	40.11	22.61	4.54	19.45	5.72	0.76	3.74	0.91	0.64	1.42	1.58	84.5
C6	31.82	22.87	5.68	28.24	5.52	1.08	2.28	1.02	0.78	0.46	1.24	79.3
C7	29.85	17.66	4.73	31.75	9.32	1.19	2.57	0.76	0.83	1.08	1.14	74.4
C8	28.80	18.37	5.69	32.08	7.29	2.72	2.59	0.38	0.78	0.88	1.67	66.8
F1	55.57	17.40	10.38	5.38	1.43	0.41	1.17	2.59	0.69	0.44	0.87	85.3
F2	52.05	14.02	5.01	11.89	4.28	0.58	3.62	2.13	0.44	0.15	1.85	92.2
F3	48.78	18.83	14.77	4.67	0.91	1.27	0.68	2.35	0.85	0.11	0.92	80.4
F4	51.61	25.91	11.22	1.72	0.95	0.10	0.37	2.31	1.17	0.24	0.73	70.9
F5	45.34	27.39	4.00	14.61	3.59	0.70	1.48	0.65	1.09	0.37	1.29	67.9
F6	59.18	25.01	9.54	1.59	0.24	0.12	0.05	3.62	0.51	0.02	1.78	75.4
F7	59.95	21.16	6.46	7.37	1.91	0.21	0.31	1.72	0.67	0.08	0.61	76.8
F8	60.46	18.65	3.97	5.64	0.41	0.28	5.62	2.62	0.55	0.00	1.37	87.2

ash systems are complex, and factors like porosity of the particle, or etch-pit style dissolution of the particle surface could result in differences in modeled results and actual system conditions. The pH dependencies, which represent the effects of OH^- on the dissolution rates, were calculated using the slopes when plotting $\log(a_{Si})$ against $\log(OH^-)$. Due to the high liquid-solid ratio, we assume that there is no significant change in pH over time during the test. The NBO/T of the fly ashes was determined using elemental compositions of amorphous contents and eq. 2:

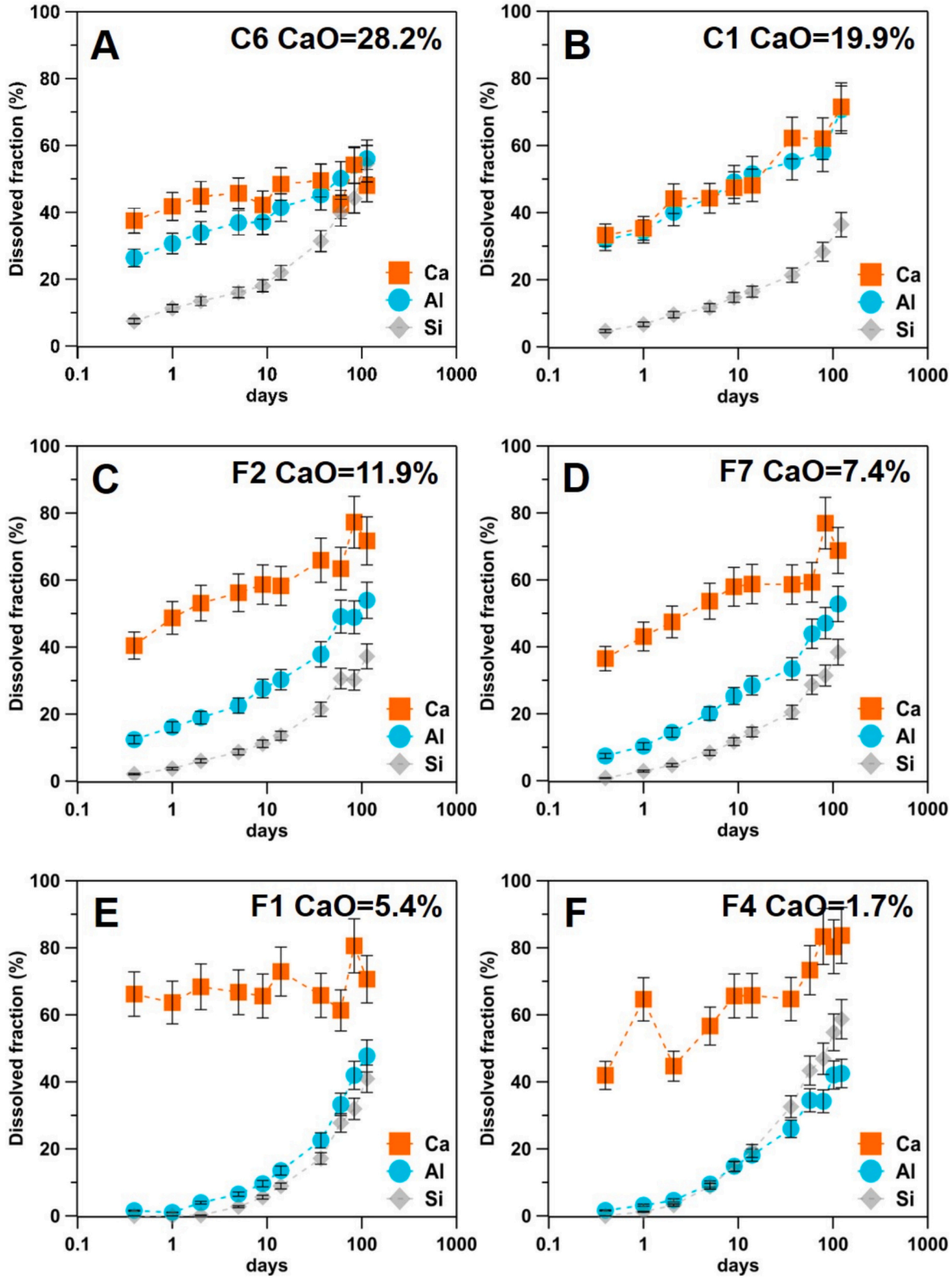


Fig. 1. The fractions of Ca, Al, and Si released during the dissolution of **(A)** C6, **(B)** C1, **(C)** F2, **(D)** F7, **(E)** F1, and **(F)** F4, at 25 °C, pH 13.1, KOH solution. The error bars show the ~ ± 10 % variability measured on selected replicate samples.

$$\frac{NBO}{T} = \frac{2\left(x_{CaO} + x_{MgO} + x_{Na_2O} + x_{K_2O} + x_{FeO} + 2x_{TiO_2} - x_{Al_2O_3}\right)}{x_{SiO_2} + 2x_{Al_2O_3}} \quad (2)$$

where x is the mole fractions of different oxides [14]. Please note that this equation is simplified, and the potential role of Al as a network modifier is not considered. The elemental compositions of amorphous phases were calculated using the XRF results and the amount and phases of crystalline components were determined by quantitative XRD analysis. The saturation indexes of potential precipitations and the estimated pH of R^3 solutions were calculated using PHREEQC and the LLNL database.

2.4. R^3 mixtures and selective dissolution

The pozzolanic reactivities of fly ashes were tested using ASTM C1897, also known as the R^3 method. A mixture of $Ca(OH)_2$, $CaCO_3$, KOH, and K_2SO_4 were used to simulate the conditions in cementitious mixtures. Samples were cured at 25, 40, and 60 °C for up to 180d, ground and oven dried at 40 °C for 24 h.

The dissolved fractions of fly ashes in the R^3 mixtures were determined using a selective dissolution method [23]. This method dissolves other solids in the dried powder and allows for quantification of the mass of residues, which are assumed to be undissolved fly ashes. 0.5 g powder were mixed with 500 mL 0.05 M EDTA solution with a pH of 11.6, adjusted by NaOH, using a bottle roller (MX-T6-S, DLAB) for 1 h. The suspensions were filtered using 0.45 μm membranes and the mass of residues was determined by drying at 110 °C for 24 h.

3. Results and discussion

3.1. Fly ash dissolution in diluted alkaline solutions

3.1.1. Stoichiometry of fly ashes dissolution

The Ca, Al, and Si released during the dissolution of 16 fly ashes in KOH solutions at pH 13.1 and 25 °C were monitored for more than 100d. The results of six fly ashes with various CaO wt% were plotted to show the stoichiometry of dissolution, i.e., the relative dissolution kinetics of different elements (Fig. 1). These six fly ashes (two ashes each of low, medium, and high CaO content) were also used in the following sections to investigate the effects of solution chemistry. The results of the other ten fly ashes are available in the Supporting Information and show similar behavior. Ca was the fastest dissolving species for most fly ashes, with 42–64 % of the Ca content released in the first day of dissolution. Ca is a known network modifier in the structure of fly ash glasses [24]. Its bonding within the framework of glasses is weaker than network formers such as Si and Al [25]. Si was the slowest dissolving species for all fly ashes, with approximately 10 % of the Si released from class C fly ashes and almost no Si released from class F fly ashes in the first day of dissolution.

The most significant difference among the fly ashes was in the dissolution of Al. For class C fly ashes C6 (28.24 % CaO) and C1 (19.91 % CaO), Al dissolution was significantly faster than Si. In contrast, Al dissolution was similar to that of Si for class F fly ashes with lower CaO contents such as F1 (5.38 % CaO) and F4 (1.72 % CaO). The higher CaO content class F fly ashes, F2 (11.89 % CaO) and F7 (7.37 % CaO), showed intermediate behavior, with Al dissolution slightly faster than Si dissolution. These observations likely suggested that either high calcium content in class C fly ashes led to the preferential dissolution of Al over Si, potentially by affecting the role of Al, shifting its function between network former and network modifier, or class C fly ashes are mixtures of fast-dissolving Ca + Al-rich phases and slow-dissolving Si-rich phases, which are consistent with observations in previous studies that groups of glass particles with varying compositions including silicates, calcium silicates, low Ca aluminosilicates, and high Ca aluminosilicates present in fly ash [26,27]. Low Ca class F fly ashes featured congruent Al and Si dissolution (Fig. 1), with steady dissolution of Si + Al-rich phases. The high-Ca class F fly ashes were a mixture of these two characteristics.

A previous study testing the dissolution of synthetic glass fly ash analogs in pH 13 KOH solutions reported similar preferential dissolution of Ca and congruent dissolution of Al and Si for glasses with CaO wt% of 15.0 and 20.0 [13]. This observation means that preferential dissolution of Al did not occur even for CaO >18 %, which differs from the observation in the current study. We suggest that the preferential dissolution of Al observed in most of the class C fly ashes in this current study could be related to greater incorporation of Al into Ca-rich and thus fast-dissolving glass content in the fly ash, leading to faster dissolution of Al than other components in the fly ash. It has been reported that particles with CaO >70 % are completely dissolved within 15 min in KOH solutions of pH 13.4 [28]. Thus, the dissolution of these Ca-rich glass contents cannot be simulated using a glass with homogenous CaO content equal to the average CaO content of the fly ash. Our observations demonstrate the challenges and limitations of using synthetic, and simplified glass phases, to represent the complex fly ash system.

The longer-term dissolution rate was found to be more congruent, as shown by the parallel curves of Al and Si for C1, F2, and F7. For C6, the dissolved Si fraction reached similar levels as the dissolved Al fraction, likely due to the consumption of reactive Al_2O_3 and the relative abundance of reactive SiO_2 content.

3.1.2. Effects of Ca, Al, and Si ions in solution on fly ash dissolution

The Ca, Al, and Si released during dissolution in our batch systems can affect the dissolution rates and extents. To elucidate their impact in our system, dissolution of Si in solutions with additions of 0.25 mM Ca, 2 mM Al, or 0.25 mM Si were compared to dissolution in the original alkaline solution. These added ion concentrations are the maximum that would not lead to precipitation based on PHREEQC calculations. The saturation indices are provided in the supporting information. The variation in dissolution rates resulting from the addition of each ion is shown relative to the original solution in Fig. 2. With the addition of Ca (Fig. 2A), the Si dissolution rates of the class C fly ashes (C1 and C6) were not significantly changed, but the class F fly ashes dissolved slower, with the reduction more evident for lower CaO content ashes. Reductions in dissolution persisted over the long term with F1 and F7 dissolving 30 % slower and F4 dissolving 50 % slower between 50 and 150 d.

Similarly, the addition of Al had no significant impact on the class C fly ashes (Fig. 2B), but dissolution for F2 and F7 was significantly reduced, with 20–50 % drop in dissolution than without the Al addition at early ages, and an average ~ 10–20 % lower over the long term. For F1 and F4, the inhibition effect was even more evident. Although the effect weakened over the long term, as much as 45–65 % reduction in silica was observed at early ages, with a 20–30 % reduction persisting up until 150d.

Increased Si (Fig. 2C) produced slight reductions in dissolution rate that increased in magnitude relative to the CaO content of the ashes, with the dissolution rate of the lowest CaO content fly ash, F4, largely unaffected, but an approximate 15 % reduction in dissolution observed for F1, F2, and F7. Dissolution of class C ashes C1 and C6 were significantly slowed, with a 20–30 % reduction across all ages. The fluctuation of the variation and the reduction in the ion effects after the early stage could be due to the heterogeneity of fly ash composition. Different fly ash particles could affect the dissolution at different stages, and could be affected by the ions differently. Further studies with detailed characterization of compositions are needed for a more accurate assessment.

In general, as more dissolution occurs and dissolved ion concentrations increase the ion activity product, Q, values (Eq. 1) will increase and dissolution rates will decrease (assuming no precipitation is occurring). One of the potential effects of adding extra Ca, Al, and Si ions is similarly increasing Q, which will cause reductions in the dissolution rates if the systems are near equilibrium. However, less than ±10 % variations in the dissolution rates of class C fly ashes with the addition of Ca and Al, as

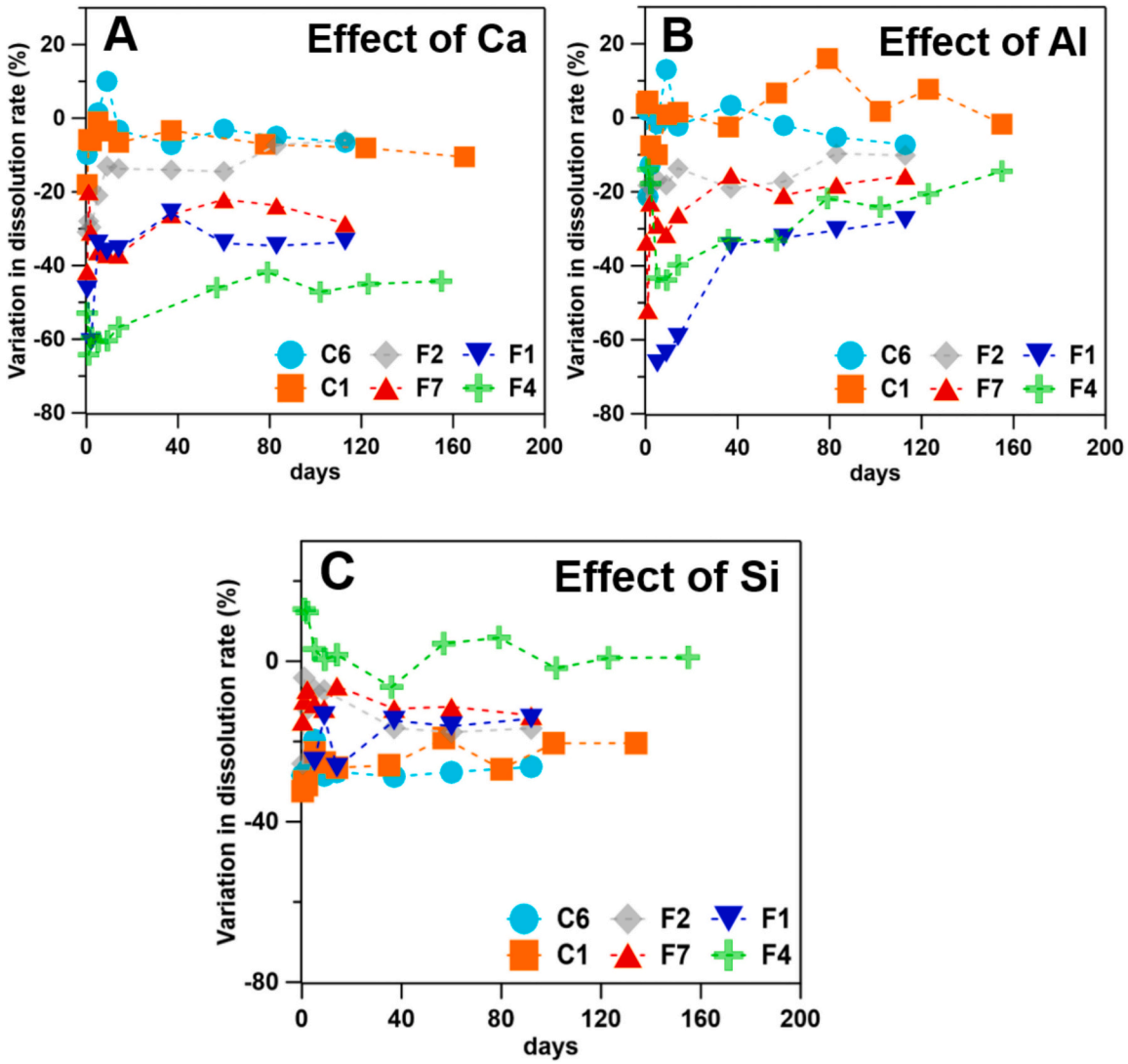


Fig. 2. The changes in Si dissolution rates of fly ashes with the addition of **(A)** 0.25 mM Ca, **(B)** 2 mM Al, and **(C)** 0.25 mM Si. Negative variation indicates reduction of dissolved Si concentration by percentage compared to the dissolved Si concentration without addition of salts. Based on the 10 % variability for dissolved ion concentrations of duplicate samples, variations in dissolution rate > 18 % can be considered as significant changes.

well as the nonsignificant impact of Si on F4 dissolution, indicates that these systems are far from equilibrium, so changes in chemical affinity of dissolution did not affect the dissolution rates. The observed inhibition effects were ion-specific and also fly ash specific, but did appear to correlate with total calcium content of the fly ashes.

Al inhibition has been observed in previous studies of aluminosilicate glasses and minerals, and suggests that the dissolution of aluminosilicate is controlled by the dissolution of reactive Si surface sites, which form by the detachment of Al [29,30]. While Si has no ion-specific effect on Si surface sites, the addition of Al led to the reattachment of Al and decreased the equilibrium fraction of reactive Si sites on particle surfaces [31]. This mechanism is consistent with the aluminosilicate phase dissolution behavior dominating the dissolution of class F fly ashes (Fig. 1E and F) and leading to inhibition of Si dissolution by increased Al in solution in class F fly ash (Fig. 2B). The observed Ca effect likely indicated that the fraction of reactive Si surface sites on class F fly ashes was decreased not only by Al but also by Ca (Fig. 2A). Based on the observed absence of Al dissolution inhibition in our class C fly ashes (Fig. 2B) and this explanation, dissolution of reactive Si surface sites does not appear to be the rate-controlling step in the dissolution of class C fly ashes. Another type of rate-controlling site may form after the initial dissolution of class C fly ashes, resulting in complexation with Si rather than Ca or Al, and explains the Si effect observed (Fig. 2C).

A previous study reported inhibition effects of Ca and Al and the absence of an effect of Si in the dissolution of synthetic glasses simulating fly ashes with 15 to 20 wt% CaO content while only Ca inhibition was observed on the Ca + Si-rich glasses simulating blast-furnace slag [13]. It was suggested that the dissolution of the fly ash glasses was controlled by the Si—O bonds, which were affected by Al in solution, and slag glass dissolution was controlled by Ca—O bonds, where Al had no effect [13]. These results were consistent with the observations on class F fly ashes in the current study, but different from the Si inhibition observed on class C fly ashes (Fig. 2C). As discussed in section 3.1.1, the CaO content of fast-dissolving phases in class C fly ashes could be much higher than the average CaO content of the ash. Thus, the single-phase synthetic glasses with 20.0 wt% CaO content may dissolve differently compared to class C fly ashes with an average CaO content of 20 %, explaining why Ca and Al inhibition instead of Si inhibition were observed in the previous study [13]. We suggest that the explanation based on Ca—O or Si—O bonds is consistent with the mechanism of reactive surface sites described above, where Si surface sites could be Si—O bonds. The absence of Si inhibition in the slag glasses observed in the previous study suggests that Ca—O bonds were not affected by Si in the solution. Considering that Si in the solution has no ion-specific effect

on Si surface sites [31], Al surface sites seem to be the only remaining option. Thus, we propose that Al surface sites are affected by Si in solution and the dissolution of Ca + Al-rich phases in class C fly ashes is controlled by Al—O bonds. As a summary, based on the different congruence of dissolution and ion effects observed in literature on synthetic glass and the class C fly ashes in this study, we suggest that fly ash particles with 20 % or less CaO content dissolve congruently with an inhibition effect from Ca and Al. Due to heterogeneity in composition, the dissolution of class C fly ash differs from the synthetic glasses with a similar average CaO contents. The high Ca particles in class C ashes dominate early-stage dissolution and are inhibited by Si ions in solution instead of Ca or Al. Further studies using synthetic glasses with high CaO content are suggested for validation.

In concrete pore solution, Al and Si concentrations are ~0.1 mM [32] and will thus affect the dissolution of fly ash in concrete less than in the systems tested here. However, dissolved Ca concentrations are known to be initially in the order of 10 mM, although decreasing to 1 mM level after 10 days [32]. Such high Ca concentrations will likely lead to the slowing of reactions of class F fly ashes. The diluted solutions used in the current dissolution tests are different from the pore solutions of concrete, but we believe the main difference will be chemical affinity and diffusion barriers formed by precipitations. The effects of aqueous species are likely due to surface adsorption and thus should apply to various conditions, similar to as is true for rate constants and activation energies (see Eq. 1). Future studies using simulated pore solutions will be needed for strict proof.

3.1.3. Effects of temperature on fly ash dissolution

Fig. 3 shows the dissolution of C1 at 25, 40, and 60 °C. The results of F1 are provided in the supporting information, which show similarly increased dissolution at higher temperature. Because the dissolution rates varied with time, the shrinking core model, shown in eq. 3:

$$\frac{kt}{R_0} = 1 - (1-\alpha)^{1/3} \quad (3)$$

where α is dissolved fraction (the ratio between dissolved Si and total Si content in fly ash), R_0 is the initial particle radius, k is a reaction rate constant dependent on solubility and interfacial kinetics and t is time, was applied to consider the reduction of surface areas due to the consumption of fly ash particles during dissolution (Fig. 3D).

For a surface reaction-controlled system, the term describing the relative completion of the reaction ($1-(1-\alpha)^{1/3}$) should increase linearly with time, and larger slope indicates faster dissolution of the particles [22]. Approximately linear relationships were observed for both C1 and F1, but at different stages with different slopes, likely due to the presence of differing glass phases with different dissolution rates present in each ash. Similar observations have been reported in a previous study on three low calcium class F fly ashes, where the dissolution was modeled in two stages: 0–28 days, where reactions were dominated by aluminosilicates; and > 28 days where stable long-term reactions were dominated by silicates [33].

Activation energies of the initial stage (α = 0–0.2) and long-term

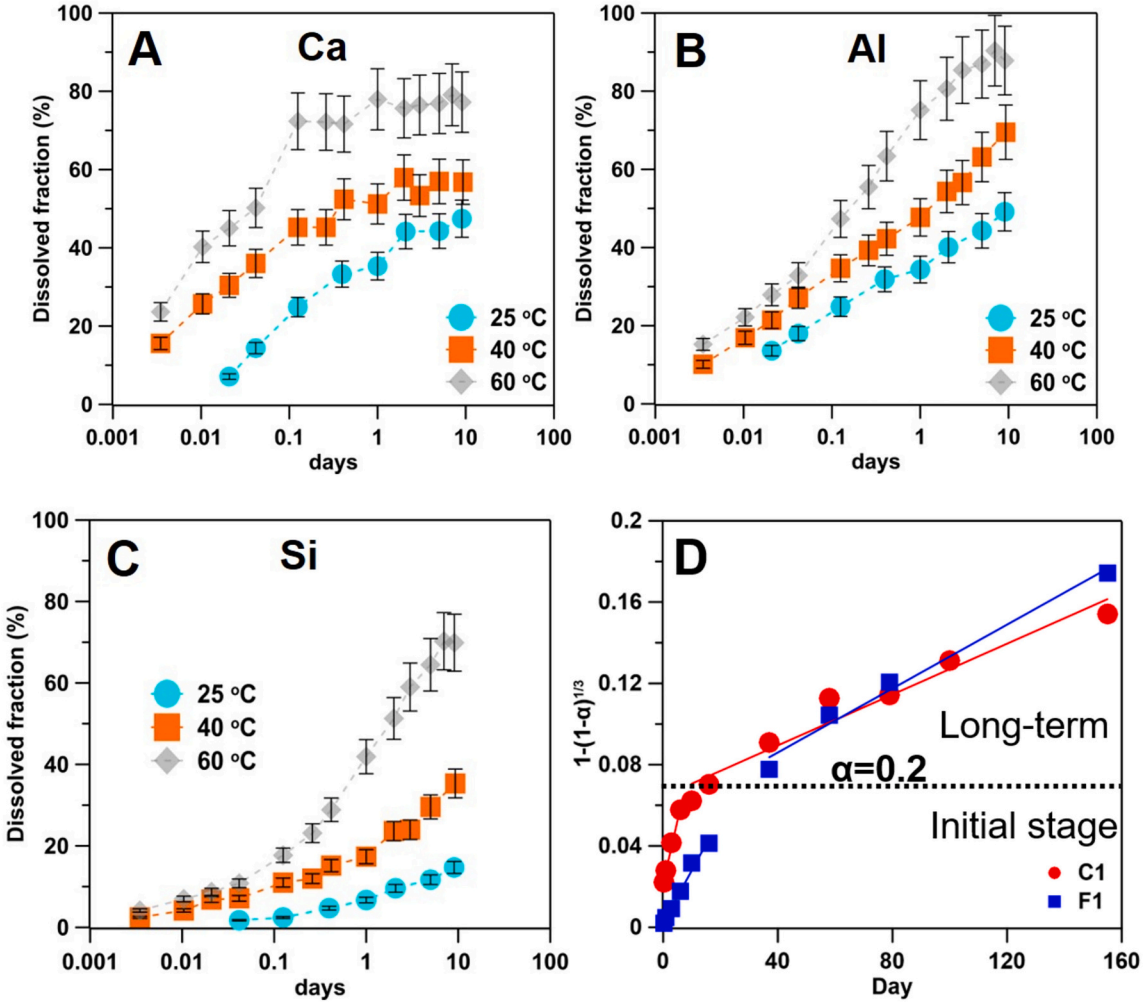


Fig. 3. The dissolved fraction of **(A)** Ca, **(B)** Al, **(C)** Si for C1 at 25, 40, and 60 °C. **(D)** $1-(1-\alpha)^{1/3}$ vs time. α is the dissolved fraction of Si at 25 °C. The solid lines in 4D are linear fittings of data at different stages. The error bars show the ~ ± 10 % variability measured for selected replicate samples.

stage ($\alpha > 0.2$) dissolution are shown in Fig. 4. The activation energies observed (56–98 kJ/mol) matched with the reported values of 67–92 kJ/mol for the dissolution of silicate minerals and glasses [34–36]. Results showed increasing activation energies for class C fly ashes and decreasing activation energies for class F fly ashes from initial stage to the long term, consistent with greater early age reactions in class C fly ashes and more sustained reactions of class F fly ashes over time.

3.1.4. pH dependency

Besides the dissolution at pH 13.1, a higher pH 13.8 and a lower pH 12.4 were also tested to understand the impact of varying pH on dissolution rates. The dissolution rates were proportional to $(a_{OH^-})^n$, where n is the pH dependency. Higher pH dependency indicates that dissolution rates are more sensitive to the changes in pH. The exponential factors, n, for the fly ashes were found to be between 0 and 0.1 at early stages (up to 5 days), indicating an increase of 0–17 % in dissolution rates for pH changes from 12.4 to 13.1 (Fig. 5A). The n gradually increased to 0.2 to 0.4 indicating 38–90 % increases with increasing pH. pH dependency ranged from 0 to 0.2 when pH increased from 13.1 to 13.8, indicating up to a 38 % increase in dissolution rates (Fig. 5B). pH sensitivity was low in both the low and high pH conditions found in concrete pore solutions, suggesting that variances in pH will not significantly affect overall fly ash dissolution.

In comparison with the fly ashes, quartz dissolution has a pH dependency of 0.3 to 0.5 [37,38], while a pH dependency of 0.4 ± 0.1 has been reported for aluminosilicate glasses at pH 9–12 [39]. In both pH ranges tested fly ash was less sensitive to changes in pH compared to quartz and previously evaluated aluminosilicate glasses, likely due to the higher pH, but more relevant to cementitious solutions, conditions used. Dissolution can become insensitive to high pH due to saturation of OH^- adsorption [40]. Considering such a weak pH effect, pH variances will not lead to large differences in overall dissolution rates of fly ashes, unless the available alkali content in the fly ash is high enough to significantly alter the system pH or the quantity of fly ash used to displace cement reaches a high enough level to significantly reduce the contribution of cement dissolution to pH development. For concrete with pore solution pH as high as 13.8, no differences in pH are expected based on the Na_2O_e content of the evaluated ashes (Table 1).

3.1.5. Na vs K

Dissolution in NaOH solutions was also tested to evaluate the impact of different alkali ions in solution on fly ash dissolution (Fig. 6A). Compared to the KOH system used in the previously discussed data, NaOH enhanced the dissolution of class F fly ashes F1 and F4. The enhancing effect was most significant in the initial stage of dissolution (up to 14 days) with an 80 % increase in dissolution for F4 and 40 % for F1. The enhancement gradually reduced to 20 % over the long term. In contrast, the enhancing effect from NaOH was not evident for the higher Ca class F fly ash F2 (11.89 % CaO), and class C fly ash C1 (19.91 % CaO). The enhancement of dissolution likely resulted from increased facilitation of depolymerization of silica by Na compared to K [1]. It has been reported that Na activators at concentrations of 4 M and 8 M are more efficient than K activators in geopolymers, a notably more extreme system, but one in which dissolution also significantly affects the rates and extents of reaction [41]. Our results show that similar mechanisms can be applied to supplementary cementitious materials in cementitious systems: even in low concentrations (0.15 M), Na increases fly ash dissolution rates more than K. The absence of Na enhancement in class C fly ashes further supported that their dissolution was controlled by different reactive surface sites.

3.1.6. Ionic strengths and sulfate

The impact of other factors in the concrete pore solution that could potentially affect fly ash dissolution, including the ionic strength (IS) and anion type (sulfate, chloride as comparison), are shown in Fig. 6. To evaluate IS, dissolution was conducted in pH 12 solutions, minimizing background IS to as low as 0.01 M. The IS was then adjusted to 0.05, 0.15, and 0.5 M using NaCl. The impact on the dissolution of C1 and F4 is shown in Fig. 6B. The changes in dissolution rates were within ±10 % for all tests, indicating that IS does not significantly affect fly ash dissolution.

The effect of the anion type on fly ash dissolution was illustrated using a potassium sulfate solution (Fig. 5C). At pH 13.1, the dissolution in 405 mM K_2SO_4 was compared to that in 810 mM KCl, which contains a similar cation concentration. Variations in dissolution rates were overall very small, suggesting no significant difference occurred as a result of anion exposure. Please note that these tests were only conducted on selected ashes, and further studies are needed to confirm the applicability to other fly ashes.

3.2. Correlation between dissolution and chemical composition

The absolute concentrations of Si released during the dissolution of six fly ashes are shown in Fig. 7A. The results of other ten fly ashes are provided in the supporting information showing similar trend. The class C fly ashes had higher dissolved concentrations before 6 days, consistent with the higher dissolved fractions shown in Fig. 1, which can be related to the more abundant network modifier, Ca, in glass structure. After 16

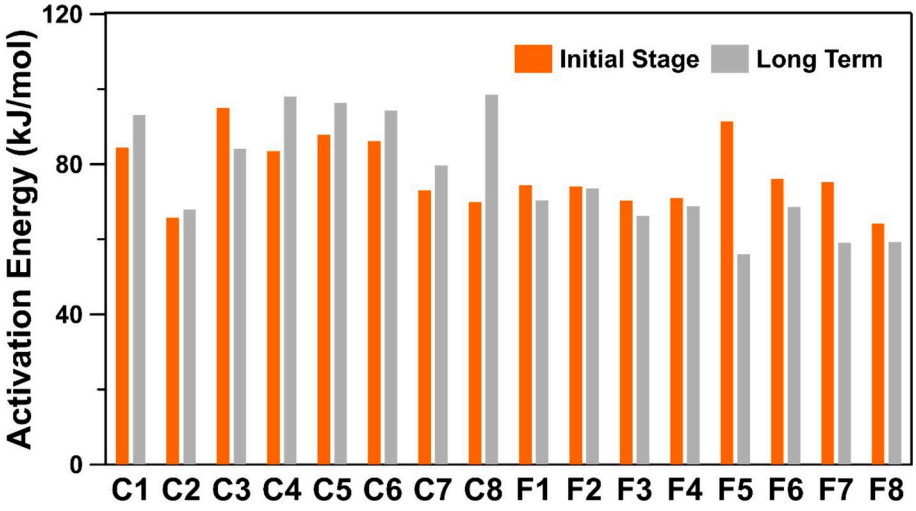


Fig. 4. Activation energy (kJ/mol) of fly ash dissolution.

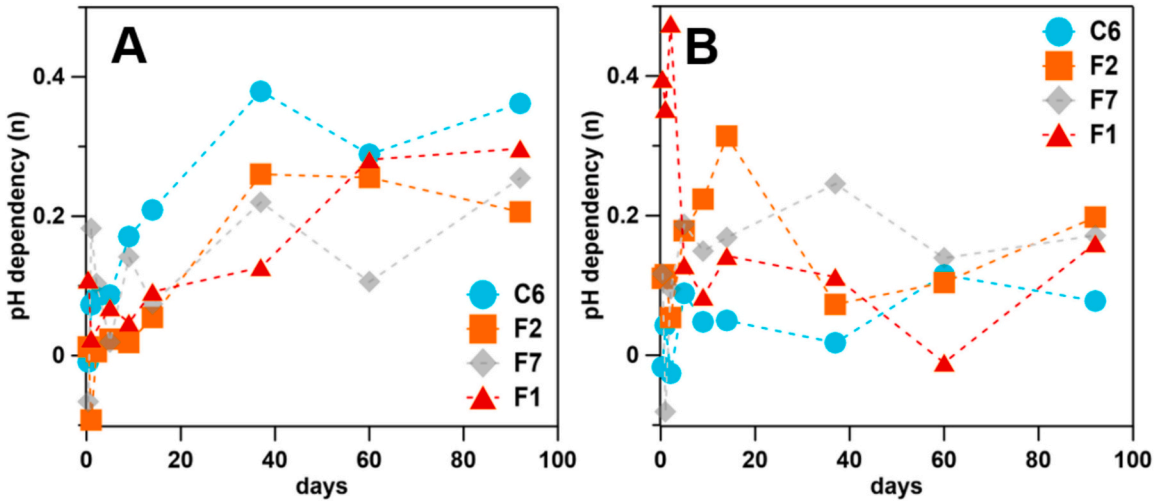


Fig. 5. The pH dependency of fly ashes dissolution at **(A)** pH 12.4 to 13.1 and **(B)** pH 13.1 to 13.8. Based on the 10 % variability for dissolved ion concentrations of duplicate samples, the error range for pH dependency is ~ ± 0.09.

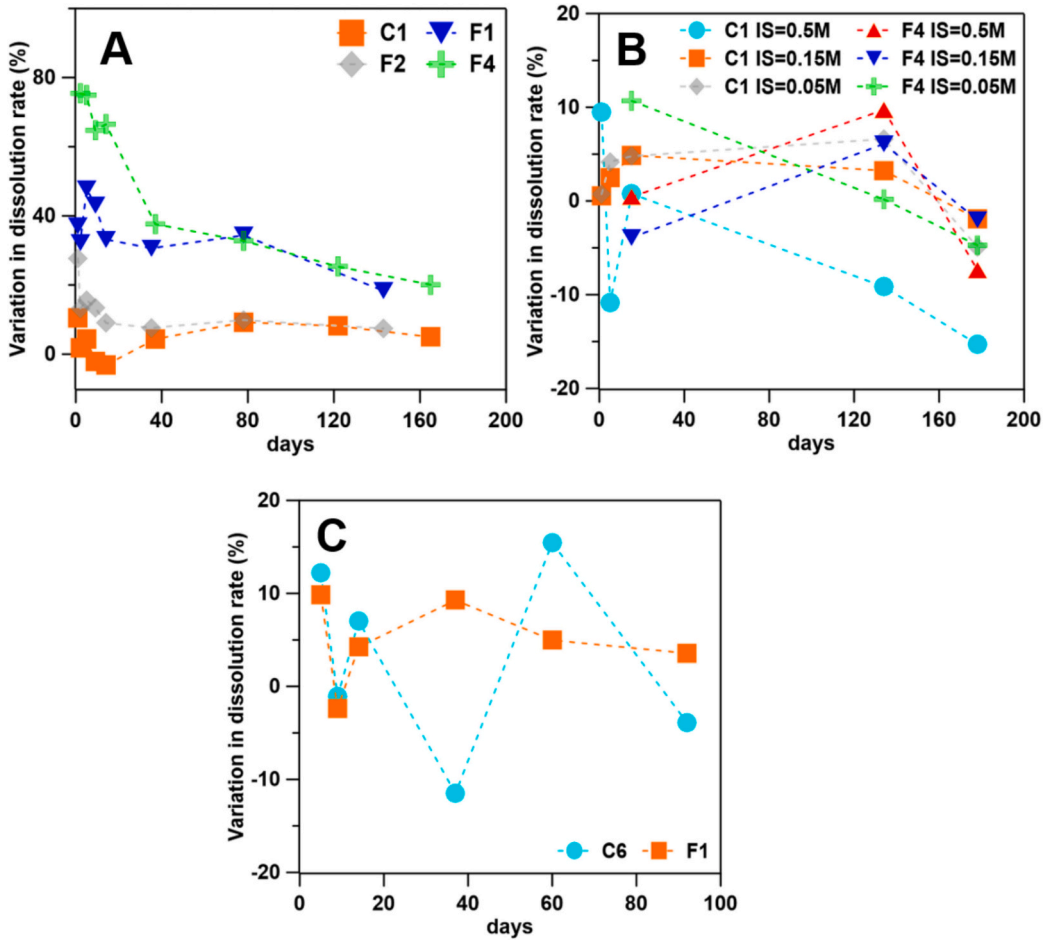


Fig. 6. The changes in dissolution rates induced by **(A)** replacing KOH with NaOH, **(B)** different ionic strength solutions, and **(C)** varying anion type using solutions of potassium sulfate in lieu of potassium chloride. Based on the 10 % variability for dissolved ion concentrations of duplicate samples, variations in dissolution rate > 18 % can be considered as significant changes.

days, the dissolution of class C slowed down likely due to the consumption of reactive silica content and class F fly ashes had higher Si concentrations owing to more persistent dissolution. These results demonstrate that the fly ash dissolution transits from glass structure-controlled in initial stage to reactive content-limited in long term.

To compare the intrinsic reactivities of different fly ashes, the dissolved Si concentrations were normalized to the surface area of each fly ash, determined using the sample particle size distribution and assuming spherical particles and a true density of 2.4 g/cm^3 for all fly ash samples. The dissolution rates were further normalized to the fraction of

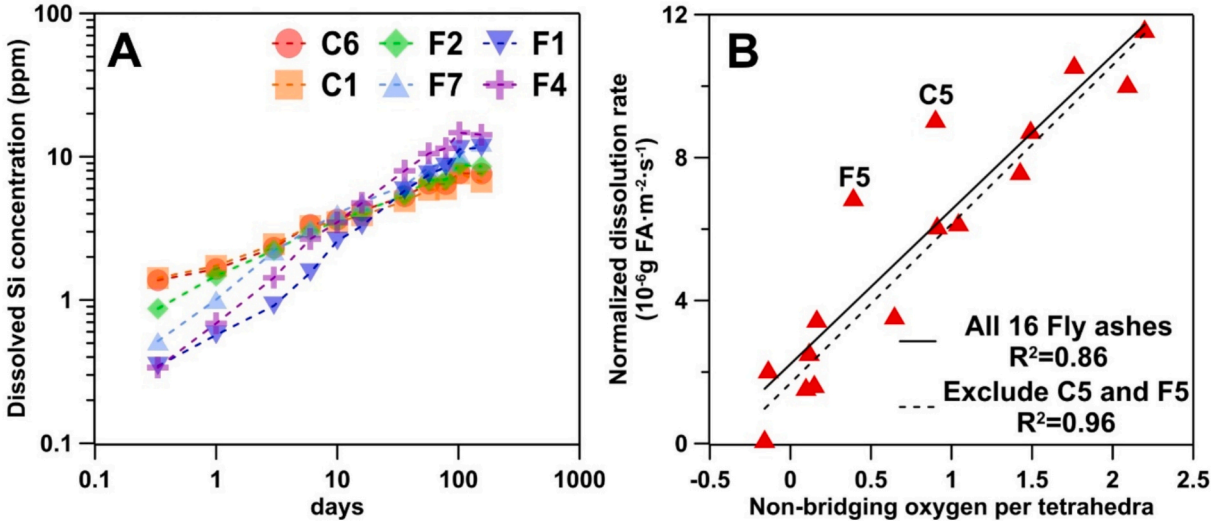


Fig. 7. **(A)** The concentrations of dissolved Si for six fly ashes at 25 °C. The error ranges are approximately ±10 %. **(B)** The correlation between the dissolution rates based on the Si released after 8 h of dissolution and the NBO/T. An R^2 of 0.86 was obtained with linear regression using all 16 samples. Without C5 and F5 (marked as outliners), the R^2 increased to 0.96 for the remaining 14 samples.

amorphous content (Table 1) and converted to fly ash dissolution constants by normalizing to the weight fraction of Si. Please note that the dissolution of crystalline phases is assumed to be minimal, which may cause certain deviations. The obtained dissolution constants were correlated to the NBO/T calculated using the oxide compositions of the amorphous content of each fly ash.

The dissolution rate at 8 h correlated well with NBO/T (Fig. 7B), with a R^2 of 0.86. The two outliers from the group, C5 and F5, were ashes with CaO contents between 14.6 and 19.4 wt%. These intermediate CaO% fly ashes are likely a mixture of Ca + Al-rich phases and Si + Al-rich phases. At 8 h, the reaction was dominated by fast-dissolving Ca + Al-rich phases, elevating overall dissolution relative to total NBO/T content in the sample. The NBO/T determined based on the averaged elemental compositions of amorphous phases will underestimate the NBO/T of the actual reacting phases in this stage. The extents of this underestimation could depend on the specific glass component and may not be accurately predicted based on average glass composition. Without these two outliers, the R^2 increases to 0.96, supporting the link between the reactivity of fly ash glasses at early ages and their glass composition.

However, cumulative dissolved Si became less well-correlated to NBO/T over time, reaching zero or negative after 6 days and indicating no relationship exists between non-bridging oxygen per tetrahedra and longer-term dissolution of the fly ashes (Table 3). Following rapid initial dissolution of their Ca + Al-rich glasses, class C fly ashes contain less Si than the class F fly ashes, leading to decreased cumulative Si dissolution in class C ashes in the long term compared to in the class F ashes. Correlations did not improve considering the total dissolved Al or the sum of Al and Si, suggesting that the presence of network disturbers such as Ca, or alkali ions can only predict the higher reactivity of class C fly ashes in initial stages, and is not related to the long-term pozzolanic reactivity or dissolution of fly ashes.

Table 3
Strength (R^2) of the correlation between dissolved Si and Al and NBO/T.

	Si	Al	Al + Si
0.33d	0.86	0.69	0.83
1d	0.84	0.66	0.80
3d	0.76	0.51	0.61
6d	0.47	0.31	0.18
10d	0.06	0.08	0.00
16d	−0.07	0.00	−0.01
36d	−0.40	−0.03	−0.07
57d	−0.43	−0.07	−0.10
79d	−0.49	−0.10	−0.12
102d	−0.58	−0.14	−0.14
155d	−0.55	−0.16	−0.15

3.3. *Dissolution in undersaturated conditions and in R^3 mixtures*

To understand how fly ash dissolution in diluted alkaline solutions compares with fly ash dissolution in cementitious mixtures used for accelerated reactivity testing, the dissolved fractions of fly ash reacted in R^3 pastes were determined using selective dissolution. R^3 mixtures simulate the saturated, high pH conditions in cementitious mixtures without the inherent variability of portland cement and attempt to evaluate long-term reactivity of pozzolanic materials through use of elevated temperatures. At 25 °C, the dissolved fractions in R^3 mixtures matched with those of our dilute KOH dissolution solutions throughout the 130-day testing period (Fig. 8), indicating that the high solid-to-solution ratios in R^3 mixtures did not inhibit the dissolution of fly ash.

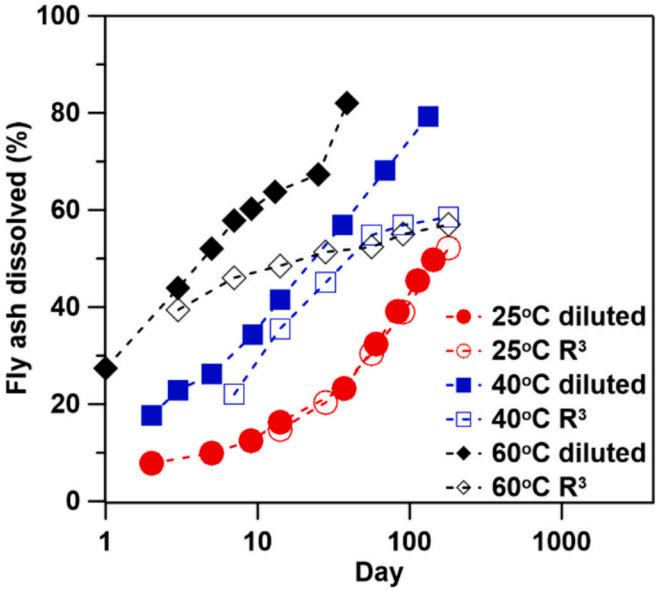


Fig. 8. The comparison between the dissolved fraction of F1 in pH 13.1 KOH solutions and in R^3 mixtures.

In contrast, at 40 and 60 °C, the dissolution of fly ash proceeded more slowly in R^3 mixtures compared to that in diluted conditions, with the disparity worsening with increasing times and temperatures. In addition, while the 40 and 60 °C dissolution tests reached >80 % total dissolution, dissolution of fly ash in the R^3 pastes plateaued at approximately 50 %. At 25 °C in the R^3 pastes, dissolution was not limited by the rate of diffusion of aqueous species across the diffusion barriers formed by precipitated phases. However, with elevated temperatures the overall kinetics of dissolution were retarded by the hydrates formed in R^3 mixtures and shifted from a dissolution-controlled process to one limited by diffusion throughout the paste microstructure. This may suggest that use of higher temperature curing, in an attempt to accelerate longer-term reactions, is changing the nature of reactions in the cementitious systems. As a result, measured reactivity of fly ashes in higher temperature systems likely underestimates the long-term overall reactivity of fly ashes in lower temperature environments as a result of, at least in part, the reduced overall dissolution of the fly ash particles.

4. Conclusions and perspective

From this work, the kinetics and influences of fly ash dissolution were evaluated. Class C ashes initially dissolve at faster rates than class F ashes, but this dominance is inverted at later ages (Table 3). After approximately 10 to 14 days, greater cumulative dissolution of Si will occur in class F systems, relative to class C, owing to the greater reactive Si content of the class F ashes. Si and Al dissolved at similar rates in low-Ca class F fly ashes suggesting the prevailing presence of aluminosilicate glass phases in class F ashes. In high Ca systems, dissolution of Al occurred preferentially over that of Si, suggesting the presence of fast-dissolving Ca + Al-rich glasses in class C ashes. Extents of preferential dissolution of Al relative to Si dissolution correlated with increasing Ca content. Class C fly ash dissolution slightly slowed with increased Si concentrations in solution, while the class F fly ashes were inhibited by Ca and Al ions in solution, and enhanced by Na compared to K. Variations in ionic strength and solution anion type (sulfate vs. chloride ions) were not observed to significantly change the kinetics of fly ash dissolution. Solution pH was shown to have little effect on fly ash dissolution, especially over the long term. The activation energies of dissolution increased for class C ashes and decreased for class F ashes between early and later stages of dissolution, reflecting known rapid reaction in class C fly ashes at early ages and greater long-term pozzolanic reaction in class F ashes.

The NBO/T was able to predict the relative rate of initial dissolution of the fly ashes, but the long-term reaction was likely limited by the reactive Al and Si content available in the fly ashes. At 25 °C, the dissolution in undersaturated and saturated conditions were similar, suggesting that the dissolution of fly ashes observed in the diluted solutions tested in this study may reflect what occurs in actual cementitious systems. At 40 and 60 °C, the reactions were slower in saturated (paste) conditions, likely due to diffusion barriers formed by hydrates different from those formed in more slowly reacting systems.

These findings reveal the varying dissolution behavior of class C and class F fly ashes and elucidate the impact of solution chemistry, temperature, and pH on fly ash dissolution. The knowledge obtained increases understanding of the relationship between the structure and composition of fly ashes and their early age reactions, controlled by dissolution kinetics. The dissolution rates, stoichiometry, activation energies, and effects of solution chemistry on the fly ash dissolution obtained here can be used to improve the kinetic database for modeling the hydration of blended cement binders. Additionally, observations herein indicate that dissolution could correlate with reactions in paste and dissolution behaviors could be used as input to accurately and simply predict fly ash's early stage and long-term reactivities. In addition, incongruence between total dissolution in the room temperature and 40 and 60 °C temperature systems suggests that use of higher temperatures to accelerate and quantify long-term reactions may underestimate the total reactivity of fly ashes used in cementitious mixtures.

In this study, we revealed the impact of temperature and chemical conditions on the dissolution of fly ashes. A major limitation is that the diluted solutions used for the dissolution test are different from the pore solution of concrete. The main difference could be that the concrete pore solution is saturated with respect to precipitation. Thus, the impact of precipitation on fly ash dissolution should be examined in the future. One effect of precipitations can be consumption of ions and continuous changes in the solution chemistry. The results on the ion-specific effects on dissolution reported here pave the pathway to accurately understand the influence of precipitation on fly ash dissolution.

We also demonstrated the transition between glass structure-controlled dissolution in the early stage to reactive content-limited dissolution in the long term. However, the pace of this transition could be different in saturated conditions due to the diffusion barriers formed by precipitation. Thus, the impact of precipitation should be addressed in future studies and combined with dissolution to fully understand the reactions of fly ashes in cementitious materials.

Lastly, we explored the differences between fly ash dissolution in diluted conditions and reaction degree in pastes using R^3 mixtures. Thus, another limitation is the potential differences between the R^3 mixture and cementitious mixtures. Further studies using cementitious mixtures are needed to understand the role of dissolution to fly ash reactivity.

CRediT authorship contribution statement

Yujia Min: Writing – original draft, Methodology, Investigation, Formal analysis. **Lisa E. Burris:** Writing – review & editing, Supervision, Resources, Funding acquisition, Conceptualization.

Declaration of competing interest

The authors declare that they have no known competing financial interests or personal relationships that could have appeared to influence the work reported in this paper.

Acknowledgments

This research was supported by Federal Highway Administration (FHWA) Exploratory Advanced Research Program grant 693JJ3-18-BAA-0001 to the project "Performance Based Classification Methods for Reclaimed Fly Ash." Coal ash materials for the research work were generously donated by Boral Materials Technologies, The SEFA Group, and Titan America.

Appendix A. Supplementary data

Supplementary data to this article can be found online at https://doi.org/10.1016/j.cemconres.2025.107967.

Data availability

Data will be made available on request.

References

[1] Z. Li, G. Xu, X. Shi, Reactivity of coal fly ash used in cementitious binder systems: a state-of-the-art overview, Fuel 301 (2021), https://doi.org/10.1016/J.FUEL.2021.121031.
[2] T. Hemalatha, A. Ramaswamy, A review on fly ash characteristics – towards promoting high volume utilization in developing sustainable concrete, J. Clean. Prod. 147 (2017) 546–559, https://doi.org/10.1016/j.jclepro.2017.01.114.
[3] ASTM, C618–19: Standard Specification for Coal Fly Ash and Raw or Calcined Natural Pozzolan for Use in Concrete, 2019.
[4] AASHTO M295: Standard Specification for Coal Fly Ash and Raw or Calcined Natural Pozzolan for Use in Concrete, American Association of State Highway and Transportation Officials, Washington DC, 2019.

[5] G. Kaladharan, A. Gholizadeh-Vayghan, F. Rajabipour, Review, sampling, and evaluation of landfilled fly ash, ACI Mater. J. 116 (2019), https://doi.org/10.14359/51716750.
[6] Y. Wang, L. Burris, R.D. Hooton, C.R. Shearer, P. Suraneni, Effects of unconventional fly ashes on cementitious paste properties, Cem. Concr. Compos. 125 (2022), https://doi.org/10.1016/j.cemconcomp.2021.104291.
[7] N.N.N. Yeboah, C.R. Shearer, S.E. Burns, K.E. Kurtis, Characterization of biomass and high carbon content coal ash for productive reuse applications, Fuel 116 (2014) 438–447, https://doi.org/10.1016/j.fuel.2013.08.030.
[8] P. Suraneni, L. Burris, C.R. Shearer, R.D. Hooton, ASTM C618 fly ash specification: comparison with other specifications, shortcomings, and solutions, ACI Mater. J. 118 (2021), https://doi.org/10.14359/51725994.
[9] Y.K. Cho, S.H. Jung, Y.C. Choi, Effects of chemical composition of fly ash on compressive strength of fly ash cement morta, Constr. Build. Mater. 204 (2019) 255–264, https://doi.org/10.1016/J.CONBUILDMAT.2019.01.208.
[10] A.K. Saha, M.N.N. Khan, P.K. Sarker, F.A. Shaikh, A. Pramanik, The ASR mechanism of reactive aggregates in concrete and its mitigation by fly ash: a critical revie, Constr. Build. Mater. 171 (2018) 743–758, https://doi.org/10.1016/J.CONBUILDMAT.2018.03.183.
[11] J. Skibsted, R. Snellings, Reactivity of supplementary cementitious materials (SCMs) in cement blends, Cem. Concr. Res. 124 (2019).
[12] S. Kucharczyk, M. Zajac, C. Stabler, R.M. Thomsen, M. Ben Haha, J. Skibsted, J. Deja, Structure and reactivity of synthetic CaO-Al2O3-SiO2 glasses, Cem. Concr. Res. 120 (2019) 77–91, https://doi.org/10.1016/j.cemconres.2019.03.004.
[13] R. Snellings, Solution-controlled dissolution of supplementary cementitious material glasses at pH 13: the effect of solution composition on glass dissolution rates, J. Am. Ceram. Soc. 96 (2013) 2467–2475.
[14] P.T. Durdziński, R. Snellings, C.F. Dunant, M. Ben Haha, K.L. Scrivener, Fly ash as an assemblage of model Ca–Mg–Na-aluminosilicate glasses, Cem. Concr. Res. 78 (2015) 263–272, https://doi.org/10.1016/j.cemconres.2015.08.005.
[15] K.L. Aughenbaugh, R.T. Chancey, P. Stutzman, M.C. Juenger, D.W. Fowler, An examination of the reactivity of fly ash in cementitious pore solutions, Mater. Struct. 46 (2013) 869–880, https://doi.org/10.1617/s11527-012-9939-6.
[16] S. Kucharczyk, M. Sitarz, M. Zajac, J. Deja, The effect of CaO/SiO2 molar ratio of CaO-Al2O3-SiO2 glasses on their structure and reactivity in alkali activated system, Spectrochim. Acta Part A Mol. Biomol. Spectrosc. 194 (2018) 163–171, https://doi.org/10.1016/j.saa.2018.01.018.
[17] S.K. Das, Yudhbir, A simplified model for prediction of pozzolanic characteristics of fly ash, based on chemical composition, Cem. Concr. Res. 36 (2006) 1827–1832.
[18] T. Oey, E.C. La Plante, G. Falzone, K. Yang, A. Wada, M. Bauchy, J.W. Bullard, G. Sant, Topological controls on aluminosilicate glass dissolution: complexities induced in hyperalkaline aqueous environments, J. Am. Ceram. Soc. 103 (2020) 6198–6207, https://doi.org/10.1111/jace.17357.
[19] J. Wang, Thermodynamic equilibrium and kinetic fundamentals of oxide dissolution in aqueous solution, J. Mater. Res. 35 (2020) 898–921.
[20] P. Aagaard, H.C. Helgeson, Thermodynamic and kinetic constraints on reaction rates among minerals and aqueous solutions; I, theoretical considerations, Am. J. Sci. 282 (1982), https://doi.org/10.2475/ajs.282.3.237, 237 LP – 285.
[21] S. Kang, Z. Lloyd, T. Kim, M.T. Ley, Predicting the compressive strength of fly ash concrete with the particle model, Cem. Concr. Res. 137 (2020) 106218.
[22] O. Levenspiel, Chemical reaction engineering, John Wiley & Sons, 1998.
[23] M. Ben Haha, K. De Weerdt, B. Lothenbach, Quantification of the degree of reaction of fly ash, Cem. Concr. Res. 40 (2010) 1620–1629.
[24] R.T. Hemmings, E.E. Berry, On the glass in coal fly ashes: recent advances, MRS Online Proc. Libr. 113 (1987) 3–38, https://doi.org/10.1557/PROC-113-3.
[25] K.-H. Sun, Fundmental condition of glass formation, J. Am. Ceram. Soc. 30 (1947) 277–281.
[26] P.T. Durdziński, C.F. Dunant, M. Ben Haha, K.L. Scrivener, A new quantification method based on SEM-EDS to assess fly ash composition and study the reaction of its individual components in hydrating cement paste, Cem. Concr. Res. 73 (2015) 111–122.
[27] T. Kim, J.M. Davis, M.T. Ley, S. Kang, P. Amrollahi, Fly ash particle characterization for predicting concrete compressive strength, Constr. Build. Mater. 165 (2018) 560–571.
[28] T. Kim, Q. Hu, M.T. Ley, M. Aboustait, J.W. Bullard, Using particle characterization to study fly ash dissolution and leaching in water and KOH solution, ACI Mater. J. 116 (2019), https://doi.org/10.14359/51716676.
[29] E.H. Oelkers, J. Schott, J.-L. Devidal, The effect of aluminum, pH, and chemical affinity on the rates of aluminosilicate dissolution reactions, Geochim. Cosmochim. Acta 58 (1994) 2011–2024, https://doi.org/10.1016/0016-7037(94)90281-X.
[30] E.H. Oelkers, S.R. Gislason, The mechanism, rates and consequences of basaltic glass dissolution: I. An experimental study of the dissolution rates of basaltic glass as a function of aqueous Al, Si and oxalic acid concentration at 25°C and pH = 3 and 11, Geochim. Cosmochim. Acta 65 (2001) 3671–3681.
[31] E.H. Oelkers, General kinetic description of multioxide silicate mineral and glass dissolution, Geochim. Cosmochim. Acta 65 (2001) 3703–3719.
[32] A. Vollpracht, B. Lothenbach, R. Snellings, J. Haufe, The pore solution of blended cements: a review, Mater. Struct. 49 (2016) 3341–3367, https://doi.org/10.1617/s11527-015-0724-1.
[33] T. Wang, T. Ishida, Multiphase pozzolanic reaction model of low-calcium fly ash in cement systems, Cem. Concr. Res. 122 (2019) 274–287.
[34] L.J. Criscenti, J.D. Kubicki, S.L. Brantley, Silicate glass and mineral dissolution: calculated reaction paths and activation energies for hydrolysis of a Q3 Si by H3O+ using ab initio methods, J. Phys. Chem. A 110 (2006) 198–206, https://doi.org/10.1021/jp044360a.
[35] Y. NIIBORI, K. Masahisa, T. Osamu, T. CHIDA, Dissolution rates of amorphous silica in highly alkaline solution, J. Nucl. Sci. Technol. 37 (2000) 349–357.
[36] T. Chida, Y. Niibori, O. Tochiyama, H. Mimura, K. Tanaka, Dissolution rate of colloidal silica in highly alkaline solution, MRS Online Proc. Libr. 824 (2004) 450–455.
[37] P.V. Brady, J.V. Walther, Controls on silicate dissolution rates in neutral and basic pH solutions at 25°C, Geochim. Cosmochim. Acta 53 (1989) 2823–2830.
[38] F.K. Crundwell, On the mechanism of the dissolution of quartz and silica in aqueous solutions, ACS Omega 2 (2017) 1116–1127, https://doi.org/10.1021/acsomega.7b00019.
[39] J.P. Hamilton, S.L. Brantley, C.G. Pantano, L.J. Criscenti, J.D. Kubicki, Dissolution of nepheline, jadeite and albite glasses: toward better models for aluminosilicate dissolution, Geochim. Cosmochim. Acta 65 (2001) 3683–3702.
[40] A.J. Gratz, P. Bird, G.B. Quiro, Dissolution of quartz in aqueous basic solution, 106–236°C: surface kinetics of "perfect" crystallographic faces, Geochim. Cosmochim. Acta 54 (1990) 2911–2922.
[41] Z. Peng, K. Vance, A. Dakhane, R. Marzke, N. Neithalath, Microstructural and 29Si MAS NMR spectroscopic evaluations of alkali cationic effects on fly ash activation, Cem. Concr. Compos. 57 (2015) 34–43.